Distortion-Robust Distributed Magnetometer for Underwater Pose Estimation in Confined UUVs

Leif Christensen, Christopher Gaudig and Frank Kirchner

Robotics Innovation Center
German Research Center for Artificial Intelligence (DFKI)
Bremen, Germany
Email: leif.christensen@dfki.de

***Abstract*—In this paper we describe a new approach to deal with dynamic distortions of the ambient magnetic field often leading to errors in orientation estimation in confined unmanned underwater vehicles. In such systems, the space to mount magnetometer sensors is strictly limited and the sensors are often in the vicinity of distortion sources like ferromagnetic material, sonar transducers or strong electric currents flowing through nearby supply lines. In our paper we describe a threefold approach to deal with these magnetic field distortions: the use of multiple distributed magnetometers for robustness, the use of very small pressure-neutral sensors to get rid of mounting restrictions inside pressure compartments and the development and application of a multi-magnetometer fusion algorithm using von Mises-Fisher (vMF) distributions to compute undistorted orientation information.**

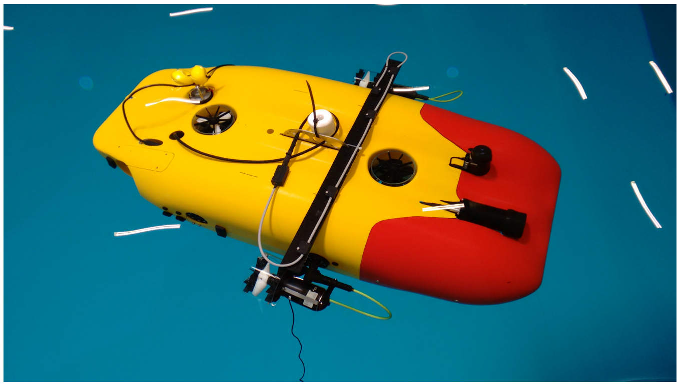

Fig. 1. The autonomous underwater vehicle *Dagon* equipped with the distributed magnetometer setup in the DFKI underwater test basin

I. Introduction

Whereas localization on the surface has found its reference technology in Global Navigation Satellite Systems (GNSS, e.g. GPS), it is not applicable in the underwater domain due to the fact that higher frequency radio signals become unusable once the sensor is submerged because of the water's strong attenuation. System solutions to the subsea localization problem are usually more expensive and, in comparison, require more custom-tailoring to the specific application scenario, usually combined with the need to set up additional infrastructure like long baseline (LBL) positioning systems or the deployment of sophisticated ultra-short baseline (USBL) setups [1].

At the base of every dead-reckoning navigation, there is commonly an inertial measurement unit (IMU), usually consisting of at least accelerometers and gyroscopes to determine orientation. Since gyroscope measurements drift over time, IMUs are often supplemented with a magnetometer to stabilize heading. The measured magnetic field is subject to significant distortions (soft and hard iron effects), caused for example by nearby ferromagnetic materials or strong electric currents. This specifically applies to compact autonomous underwater vehicles and robots, where mounting options for magnetometers inside pressure housings are strictly limited. Depending on the severity of the system-induced and dynamically changing field distortions in the vicinity of the sensor, a-priori calibration techniques can correct the measurements only to a certain point and may fail completely on systems with moving ferromagnetic parts (for example underwater gliders with moving battery packs).

In our paper we describe a threefold approach to deal with these magnetic field distortions: *a*) the use of multiple distributed magnetometers for robustness *b*) the use of very small pressure-neutral sensors to get rid of mounting restrictions inside pressure compartments and *c*) the development and application of a multi-magnetometer fusion algorithm using von Mises-Fisher (vMF) distributions [2] to compute undistorted pose information.

Since dynamic distortions of the magnetic field are usually locally distributed (e.g. near turning permanent magnets of a motor or near current supply lines), we can show that applying our vMF-based fusion algorithm to the distributed magnetometer measurements enhances the overall robustness and performance of the heading filter solution.

II. Distributed Magnetometer Hardware Setup

In the current setup, five very small and inexpensive magnetometers (ST LSM303D) and one microcontroller (Atmel ATmega 644P) are individually moulded in polyurethane casting compound, resulting in a single cable whip (see fig. 2) which can be easily and freely distributed outside the underwater vehicles' pressure housings.

Although most of the electronic parts on the microcontroller board are pressure resistant due to their SMD package type,

978-0-933957-43-5 ©2015 MTS

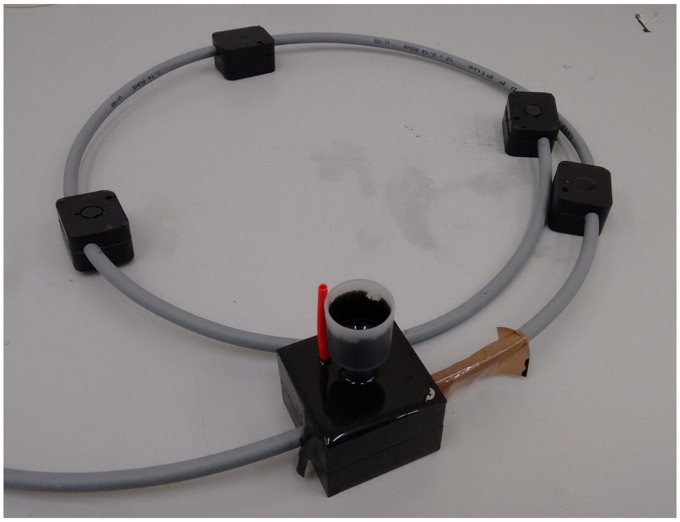

Fig. 2. Moulding of distributed magnetometers using polyurethane casting compound

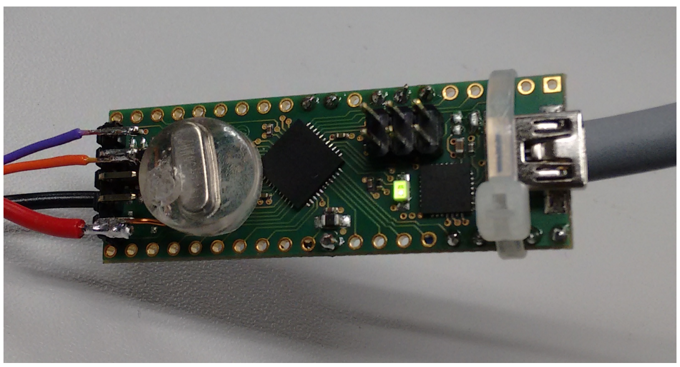

Fig. 3. Epoxy-infused crystal oscillator

special care had to be taken of the hermetically sealed crystal oscillator providing the system's clock-signal to avoid collapse under high pressure [3]. Since the polyurethane is still quite flexible after curing (which is necessary to allow for a good and flexible bond with the cable), it is possible that the polyurethane would exert pressure on the crystal oscillator package. This would prevent the crystal from oscillating freely in a high pressure surrounding, resulting in wrong clock frequencies or even fatal damage of the oscillator. Therefore, the package was sealed separately in epoxy resin, which is less compressible than the polyurethane (see fig. 3).

To avoid inner tension in the epoxy which could lead to cracks in the material, microballoons (hollow glass microspheres) were added to the epoxy casting compound, preventing the exertion of pressure on the oscillator housing during the curing process. The cast microcontroller module was integrated directly into the cable to avoid the integration of another housing (fig. 4).

The ST LSM303D type of MEMS magnetometer that was used in this work can be interfaced using either I^2C or SPI. I^2C would have been the obvious choice due to the smaller amount

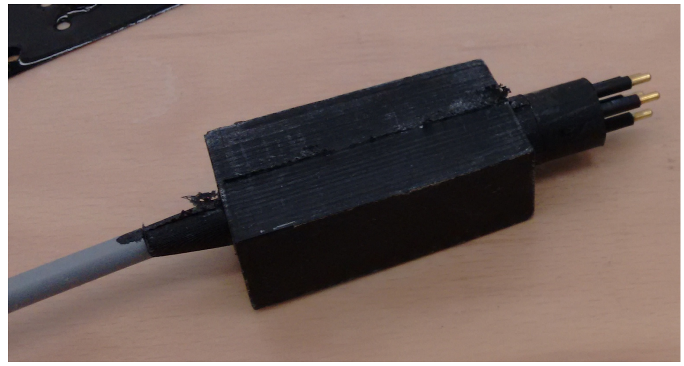

Fig. 4. Microcontroller integrated with industry standard underwater plug

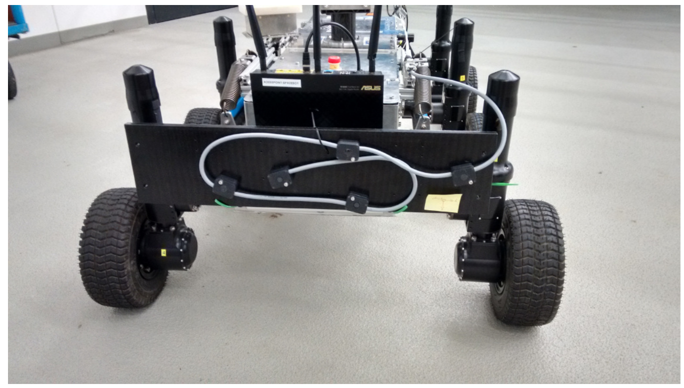

Fig. 5. Distributed magnetometer on the *Artemis* Rover during experiments

of signal wires, but since the magnetometer only allows two different I^2C slave addresses which would have required the integration of an additional multiplexer, we opted for SPI in our scenario.

III. Distributed System Deployment

The described distributed magnetometer setup was first deployed on a land-based robotic system (*Artemis*, see [4] for an in-depth description) and later installed on unmanned underwater vehicles (crawler *Wally* and hybrid AUVs *Dagon* and *FlatFish*).

A. Wally

The Wally crawler was designed to investigate the seabed of the Neptune Canada Observatory at the Barkley Canyon methane seep site. The crawler is equipped with a new methane sensor to monitor the flux of methane into the water from the sediments, and a new side-mounted camera for the development of an automated 3D mapping and photogrammetry system in conjunction with DFKI ROBEX partners. The crawler is intended for longer periods of autonomous operation [5].

B. Dagon

The Dagon AUV is specifically designed as a scientific AUV for visual mapping and localization. Its high-quality stereo

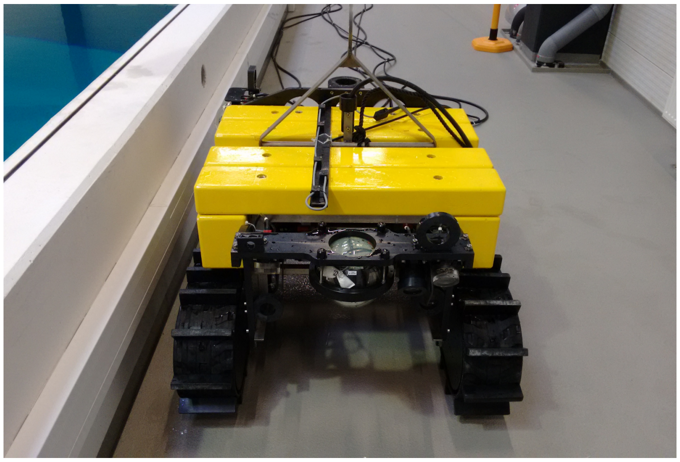

Fig. 6. The underwater crawler *Wally* in the DFKI underwater test basin

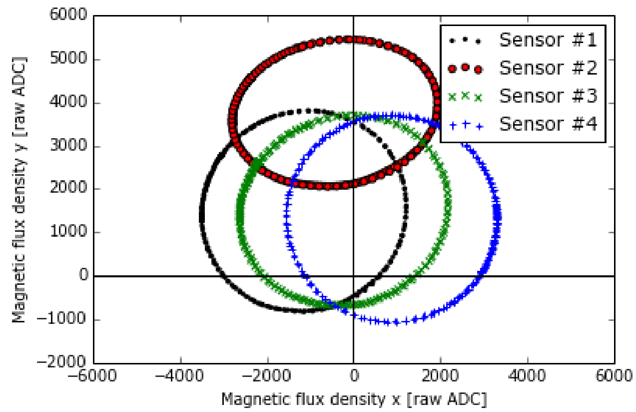

Fig. 7. Hard-iron distortion and sensor misalignment on robotic crawler *Wally* magnetometer readings projected onto the xy-plane leading to off-center effects of different strength, depending on mounting position on the vehicle

camera system acts as the main sensor system for this application and is supplemented by the internal IMU and pressure sensor. Using visual odometry and SLAM approaches, a map of the seafloor and the vehicle's trajectory is generated [6].

In order to validate the measurements produced by this visual approach to mapping and localization, the AUV's additional navigation instrumentation (LBL, DVL, FOG) allows a second independent measurement to be recorded employing widely used and proven algorithms. This second measurement can be used as a ground truth for the performance evaluation of new navigation techniques. The AUV has a nominal operating time of six hours, which may vary with the type of mission. It can either be used as a completely autonomous vehicle, with the only communication available being the low-bandwidth acoustic modem, or connected to a fiber-optic cable for telemetry. Using this cable, a hybrid-ROV mode is also possible, where the vehicle is controlled by a human operator or a control station on shore [7].

C. *FlatFish*

The *FlatFish* AUV serves as a shallow water ($<$ 300m) inspection platform, intended for collecting camera, sonar and laser line data of underwater structures and pipelines [8]. It is equipped with six hubless ring thrusters providing a force of 60N each, thus being able to actuate all but its roll axis. The drives are supplied with the battery voltage (ranging from 42V to 59V depending on state-of-charge) and have a full-speed design current of 8A each. The 5.8 kWh battery is located at the very rear of the AUV, away from the magnetometer setup.

IV. Algorithm

A. *Magnetic Field Distortions*

1) Geomagnetic Field Distortions: A compass application for heading estimation depends on measuring the horizontal components of the earth's magnetic field to determine the direction towards the magnetic north pole. Although the pole's location is changing over time (and picking up speed) and the magnetic field is significantly locally distorted depending on latitude and longitude of the observer, the declination from magnetic to true north can be computed using analytical models like the *World Magnetic Model* (WMM) [9] or the *International Geomagnetic Reference Field* (IGRF) [10] and there are even numerical models for geomagnetic field reversals [11]. Apart from this variation coming from the main magnetic field density contributors (the earth core (geodynamo effect) and the earth crust), the earth magnetic field can be considered locally static for our purpose. However, there are also variations due to changes in the magnetosphere coming from SQ-Variations or coronar mass ejections (CME), but even magnetic storms classified as a "Super Storm" only have a very slight impact (orders of magnitude lower, typically less than 250 nT) on the overall earth magnetic field strength (around 49,400 nT in Northern Germany).

2) System-immanent distortions: Apart from the distortions of the geomagnetic field, one has to also consider the distortions created by the vehicle itself. Ferromagnetic materials or strong currents flowing through a wire in the vicinity of the sensors can cause significant distortions of the measured magnetic flux density. These vehicle-immanent distortions are usually classified as hard- and soft-iron effects [12]. Hard-iron effects occur due to the magnetic remanence of nearby material (permanent magnets in motors, magnetized iron or steel) and show a constant offset in every field component measured at the sensor position. Without distortions, plotting directions on an S^2 sphere in $\mathbb{R}^3$ would result in measurements of arbitrary direction having the same distance to the origin. Hard-iron distortions however lead to a shift of the center of the sphere from the origin (see fig. 7) and can be modeled as a 3-component bias vector b_{hi} (one-cycle error):

$$b_{hi} = \begin{pmatrix} x_{hi} & y_{hi} & z_{hi} \end{pmatrix}^T$$

.

Please note that strong currents flowing through wires near the magnetometers also lead to a hard-iron effects, but are usually non-static. How we deal with these non-static distortions is described in IV-C.

Soft-iron effects distort the magnetic field by providing a path of lower impedance while an external field is applied to the ferromagnetic compound. This induces magnetism depending on the orientation of the material with respect to the applied (geomagnetic) field (two-cycle error). As such, soft-iron effects lead to deforming the sphere to an 3D ellipsoid, but retaining the origin. The soft-iron effects can be described by a $3x$ matrix M_{si}:

$$M_{si} = \begin{pmatrix} m_{11} & m_{12} & m_{13} \\ m_{21} & m_{22} & m_{23} \\ m_{31} & m_{32} & m_{33} \end{pmatrix}$$

Once these values are determined in a calibration procedure, the static part of the system-immanent hard- and soft-iron effects can be compensated (see section IV-B below).

B. Static calibration

Before we can apply our vMF-based filter to compensate dynamic distortions of the measured magnetic flux density field, we have to account for the static vehicle hard- and soft-iron distortions. In order to get calibrated sensor readings $\hat{x}, \hat{y}, \hat{z}$ from raw sensor readings x, y, z, we have to apply the following equation:

$$\begin{pmatrix} \hat{x} \\ \hat{y} \\ \hat{z} \end{pmatrix} = M_{align} \cdot \begin{pmatrix} sc_x & 0 & 0 \\ 0 & sc_y & 0 \\ 0 & 0 & sc_z \end{pmatrix} \cdot M_{si} \cdot \left(\begin{pmatrix} x \\ y \\ z \end{pmatrix} - b_{hi} \right)$$

with the misalignment matrix M_{align}, a diagonal scale matrix SC, soft-iron distortion matrix M_{si} and offset vector b_{hi}, which incorporates hard-iron distortions as well as sensor-immanent ADC offset errors. As stated previously, undistorted or perfectly compensated magnetic field flux density readings would cover the surface of an origin-centered sphere, while hard- and soft-iron distortions as well as sensor errors lead to an off-centered ellipsoid, which can be modeled as a second-order algebraic surface:

Not taking cross-axis effects into account, we can describe our ellipsoid as

$$\frac{(x - x_{hi})^2}{a^2} + \frac{(y - y_{hi})^2}{b^2} + \frac{(z - z_{hi})^2}{c^2} = R^2$$

In order to apply least-squares ellipsoid fitting methods to discover the correction parameters for hard- and soft-iron distortions, sensor bias and scaling, we rewrite this equation to

$$\begin{pmatrix} x & y & z & -y^2 & -z^2 & 1 \end{pmatrix} \cdot X = x^2$$

with

$$X = \begin{pmatrix} 2x_{hi} \\ \frac{a^2}{b^2} 2y_{hi} \\ \frac{a^2}{c^2} 2z_{hi} \\ \frac{a^2}{b^2} \\ \frac{a^2}{c^2} \\ a^2 R^2 - x_{hi}^2 - \frac{a^2}{b^2} y_{hi}^2 - \frac{a^2}{c^2} z_{hi}^2 \end{pmatrix}$$

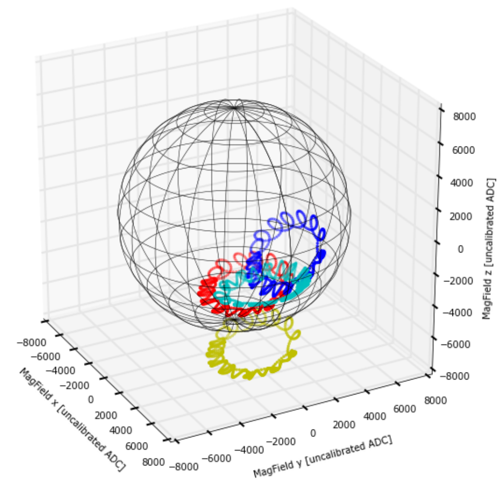

Fig. 8. Scatter plot of uncalibrated ADC magnetometer readings of sensors #1-#4 on robotic crawler *Wally* during static calibration procedure

which is our linear equation system

$$H \cdot X = w = x^2$$

to put into the least-squares solver.

A set of uncalibrated values of x, y and z would ideally be sampled from every sensor in the multi-magnetometer array in a distortion-free magnetic field environment and evenly cover the full space of 3D directions. Unfortunately, we cannot do full-circle turns in every vehicle axis (roll, pitch and yaw), since this would involve either sophisticated and huge gimbals for the systems in air or powerful thrust under water, if even possible at all (crawler systems). Also, this would induce non-static contortions. But since our model is already restricted to a quadratic ellipsoid surface, we saw that doing a full 360° yaw circle involving roll and pitch movement from -20° to +20° is sufficient to recover the ellipsoid form from the uncalibrated data (see fig. 8). We conducted this turn-and-wiggle motion as far away from any steel structure as possible while being attached to a crane on a 6m polyester hoisting sling.

After solving for the combined scale matrix SC and soft-iron distortion matrix M_{si}, as well as the combined sensor bias and hard-iron offset vector b_{hi}, only the misalignment matrix M_{align} has to be established.

For this we carried out several flat turns around the yaw axis with the AUVs *Dagon* and *FlatFish* as well as the crawler *Wally*, in an utmost undistorted environment, this time avoiding any roll and pitch movements.

Apart from small non-orthogonalities in the sensors themselves, the misalignment matrix is basically a rotation matrix that turns the sensor frame to the fixed body frame of the

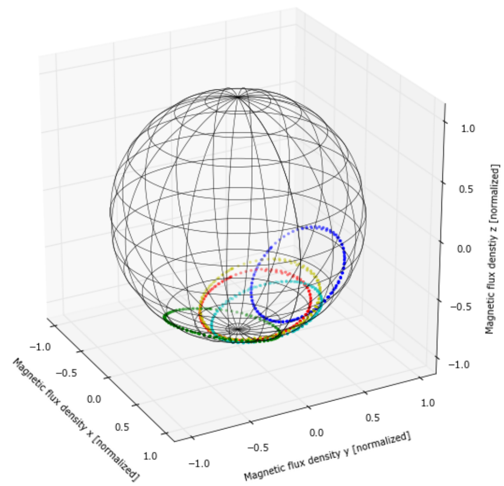

Fig. 9. Scatter plot of compensated but still unaligned magnetometer readings of sensors #1-#5 on AUV *Dagon* during the static calibration procedure (flat turns around yaw axis

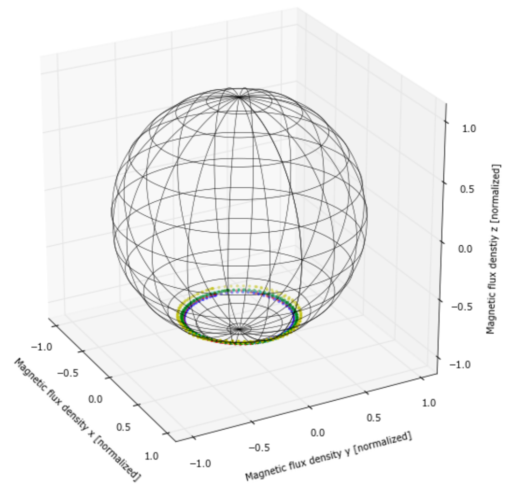

Fig. 10. Scatter plot of compensated and aligned magnetometer readings of sensors #1-#5 on AUV *Dagon* during the static calibration procedure (flat turns around yaw axis

vehicle. Since a rotation can be described with a minimum of 3 degrees of freedom, direct least-squares solving for all 9 values of the 3x3 rotation matrix would not result in a pure rotation matrix. We therefore use Rodriguez' rotation formula

$$\mathbf{v}_{\mathrm{rot}} = \mathbf{v}\cos\theta + (\mathbf{k} \times \mathbf{v})\sin\theta + \mathbf{k}(\mathbf{k} \cdot \mathbf{v})(1 - \cos\theta)$$

which rotates a vector $\mathbf{v}$ around a unit vector rotation axis $\mathbf{k}$ by an angle of θ resulting in $\mathbf{v}_{\mathrm{rot}}$ and least-squares solve for $\mathbf{k}$ and θ with $\mathbf{v}$ being the distortion-compensated sample from the flat turn around the vehicle's z-axis and $\mathbf{v}_{\mathrm{rot}} = \begin{pmatrix} 0 & 0 & -1 \end{pmatrix}^T$. From that we can compute our misalignment matrix M_{align}:

$$\mathbf{M}_{\mathrm{align}} = \mathbf{I} + (\sin\theta)\mathbf{K} + (1 - \cos\theta)\mathbf{K}^2$$

with

$$\mathbf{K} = \begin{bmatrix} 0 & -k_3 & k_2 \\ k_3 & 0 & -k_1 \\ -k_2 & k_1 & 0 \end{bmatrix}$$

Putting everything together, figure 9 and figure 10 show the compensated and compensated+aligned magnetometer readings on the AUV *Dagon* respectively. Figure 11 shows the result of the static calibration and misalignment computation for the crawler *Wally*, projected onto the xy plane.

C. Dynamic Distortion Filtering

Apart from *static* distortions local to the vehicle, which are accounted for by an a-priori calibration procedure (see IV-B), the local *dynamic* distortions have to be compensated online.

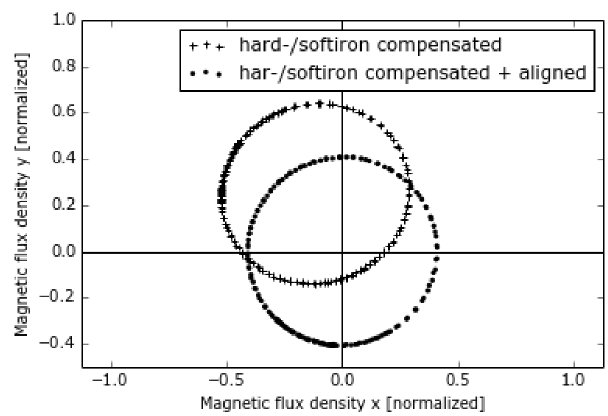

Fig. 11. Scatter plot of magnetometer readings of sensor #1 on robotic crawler *Wally* projected onto the xy-plane after hard- and soft-iron as well as misalignment compensation

In this work we filter out these dynamic effects by means of multiple small sensors freely distributable on the vehicle. This makes it not only possible to mount the sensors farther away from the distortion source than a single large high-precision IMU, but since the dynamic distortions of the magnetic field are usually locally distributed and show up only in a subset of the sensors (for example near motor current supply lines), this also allows us to apply statistical filtering. Another approach we are pursuing to deal with these dynamic distortions (especially in complex robot setups with multiple moving ferromagnetic parts) is to apply machine learning techniques like Support Vector Regression (SVR) to learn the distortion functions. While the latter shows promising results in case there is realtime data available on the internal robot state (posture, motor currents, etc.), we concentrate on the filtering approach in this work, since it allows to deal with dynamic distortions as an add-on system, even if one has no interface to the internal data of the vehicle at hand.

1) vMF Distribution: Since the magnetic field is a vector field, dynamic distortions have an effect both on the magnetic flux density (strength component) as well as on its direction. Sometimes even strong distortions only result in a variation of the field strength (maintaining the direction), while other distortions don't change the magnetic field strength, but result in large direction deviations. To determine how strongly one sensor in the array is disturbed with respect to the rest of the magnetometer sensors on the vehicle, we use the probabilistic density functions of two different 3-dimensional multivariate probabilistic distributions. We are interested in the probability of a measurement $\mathbf{x}_i$ of sensor i given a set of measurements of the rest of the sensors.

We model the strength component as a Gaussian distribution of the $L2$-norm with mean μ_{st} and standard deviation σ. The probability density function for the strength component is therefore defined as

$$p(\mathbf{x}_i|\mu_{st},\sigma) = \frac{1}{\sigma\sqrt{2\pi}}\, e^{-\frac{(x-\mu_{st})^2}{2\sigma^2}}$$

To model the three-dimensional direction component, we use the *von Mises Fisher* (vMF) distribution [2], originating from directional statistics work, analog to circular wrap-around distributions in the one-dimensional case.

The vMF distribution is defined on the S^{p-1}-dimensional sphere in $\mathbb{R}^p$. The probability density function of a vMF distribution on S^2 is given by

$$p(\mathbf{x_i}|\mu_{dir},\kappa) = \frac{\kappa}{4\pi\sinh\kappa}\exp(\kappa\mu_{dir}^T\mathbf{x_i})$$

with mean direction μ_{dir} and concentration parameter κ for a unit direction vector $\mathbf{x}$. In case of $\kappa = 0$, the distribution is uniform while it is more concentrated with higher κ (see fig. 12). We approximate μ_{dir} as

$$\hat{\mu}_{dir} = \frac{\mathbf{r}}{\|\mathbf{r}\|} = \frac{\sum_{i=1}^{n}\mathbf{x_i}}{\|\sum_{i=1}^{n}\mathbf{x_i}\|}$$

and κ according to [13] and as proposed for small dimensions by [14] as

$$\hat{\kappa} = \frac{\bar{r}d - \bar{r}^3}{1-\bar{r}^2}$$

with

$$\frac{\|\mathbf{r}\|}{n} = \bar{r}$$

Combining both strength and direction components we can now determine the probability of a measurement $\mathbf{x}_i$ of sensor i given the current Gaussian and vMF distribution as

$$p(\mathbf{x}_i|\mu_{st},\sigma)p(\mathbf{x}_i|\mu_{dir},\kappa)$$

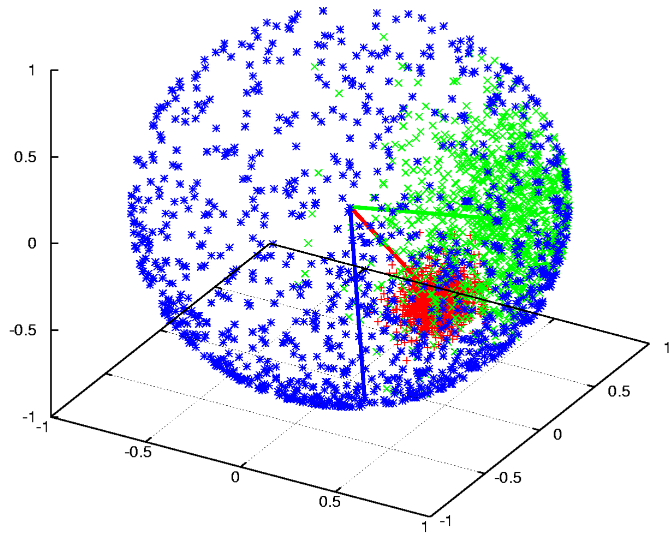

Fig. 12. Samples from three different vMF-distributions on S^2 with different mean and $\kappa = 1$(blue), $\kappa = 10$(green) and $\kappa = 100$(red). Image courtesy of Wikipedia.

2) Filter Implementation: Now that we can compute the probability of the current measurement $\mathbf{x}_i$ of sensor i in the sensor array, we give a weight w_i according to its probability to every measurement $\mathbf{x}_i$, so that measurements strongly deviating from the rest of the measurements influence the result less.

function DYNAMIC_FILTER
    for $i \leftarrow 1$ **to** n **do**
        $\mathbf{x}_i \leftarrow readout\_magnetometer(i)$
    end for
    $\mu_{st},\sigma \leftarrow$ mean and std of strength (L2 norm)
    $\mu_{dir},\kappa \leftarrow$ mean and concentration parameter of vMF distribution
    $w_i \leftarrow p(\mathbf{x}_i|\mu_{st},\sigma)p(\mathbf{x}_i|\mu_{dir},\kappa)$
    return normalized weighted sum of $\mathbf{x}$
end function

The result can either be used standalone as the normalized weighted sum or each sensor can be integrated as a single measurement in a higher level sensor fusion algorithm (e.g. EKF orientation estimator) with per-sensor confidence values according to the computed weight.

D. Results

Experiments to validate the approach were conducted on the unmanned underwater crawler *Wally* and the hybrid AUVs *Dagon* and *FlatFish*) at the DFKI underwater robot test facilities. Several data acquisition runs were carried out, amongst them static setups, straight driving, circling and wall following.

Figure 13 shows the calculated heading of sensors 0-4 after static calibration during a manually steered straight run in the DFKI underwater test basin of 1.5 minutes duration. Also plotted is the heading calculation of a high-precision fiber optical gyroscope (FOG) as reference. As can be seen, strong

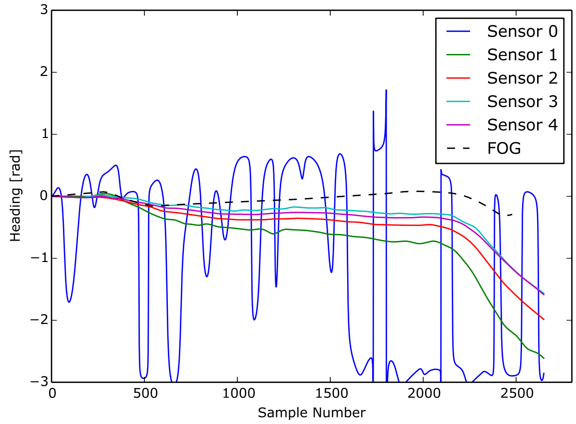

Fig. 13. Calculated heading of single sensors after static calibration during *Dagon* straight run in the DFKI underwater test basin

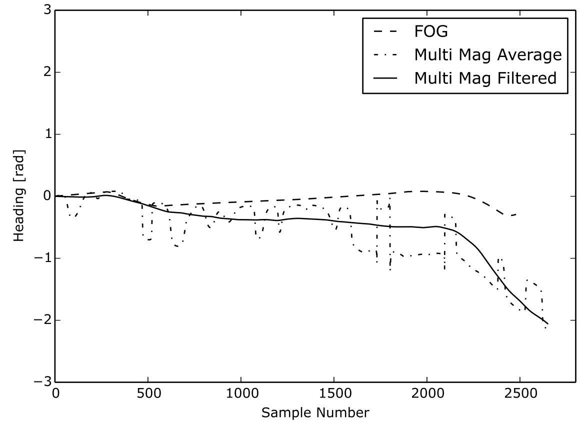

Fig. 14. Comparison of averaged and proposed dynamical filtering of the magnetometer array readings during *Dagon* straight run in the DFKI underwater test basin

dynamic distortions occur in sensor number 0, assumedly due to the mounting position near a sonar transducer. Please note that the proposed hardware setup of the multi-magnetometer system (with the availability of several sensors at different positions outside the pressure hull and farther away from possible disturbance sources) already allows for much less distorted magnetometer readings of other sensors (here sensors 1-4).

Figure 14 shows the performance of the proposed method in the presence of local dynamic distortions as they are expected to appear on confined UUVs, in this case on the AUV *Dagon*. As can be seen, although there still is a divergence between the reference FOG-heading and the filtered solution using the presented approach, the proposed dynamic filter using vMF-distributions performed better as an averaging-filter due to the algorithmic design, which in this case assigns a low weight to the deviating sensor 0 with respect to the rest of the sensors (1-4).

V. Conclusion

In this paper we described a new approach to deal with dynamic distortions of the ambient magnetic field often leading to errors in orientation estimation in confined UUVs. We proposed a small distributed and pressure-neutral sensor array design to remove mounting restrictions. It was successfully interfaced with several different robotic underwater systems and was evaluated on three of them at the DFKI underwater test facility. To improve the robustness of magnetometer / compass readings we applied a new multi-magnetometer fusion algorithm using von Mises-Fisher (vMF) distributions and showed its performance in the presence of strong local vehicle distortions.

To further enhance the robustness of magnetometer readings on confined robotic systems in the future, we will look into using the Fisher-Bingham / Kent distribution instead of the vMF distribution in order to better account for per-axis dispersion on the unit sphere. We have already evaluated how to use distortions of the ambient magnetic field surrounding the robot for position estimation and mapping and will apply the approach described in this paper to that area. Another promising approach we started examining is to learn the dynamic magnetic field distortions of a system using Support Vector Regression techniques for cases where enough data on the internal state of a robot is available.

Acknowledgment

The authors would like to thank all colleagues at the DFKI Robotics Innovation Center, especially Sascha Arnold, Alexander Duda, Andre Gerdes, Stefan Haase, Marc Hildebrandt and Jakob Schwendner for their support and feedback. The research leading to this result has received funding from the European Union Seventh Framework Program under the joint research activity of the EUROFLEETS2 project (grant No. 312762) and the German Federal Ministry of Economics and Technology (BMWi), project TransTerrA (grant No. 50RA1301).

References

[1] L. Christensen, M. Fritsche, J. Albiez, and F. Kirchner, "USBL pose estimation using multiple responders," in *Proceedings of OCEANS 10 IEEE Sydney. OCEANS MTS/IEEE Conference (OCEANS-10), Showcasing Advances in Marine Science and Engineering, May 24-27, Sydney, Australia*, 5 2010.

[2] R. A. Fisher, "Dispersion on a sphere," in *Proc. Roy. Soc. London*, ser. A, vol. 217, 1953, pp. 295–305.

[3] P. Kampmann, J. Lemburg, H. Hanff, and F. Kirchner, "Hybrid pressure-tolerant electronics," in *Proceedings of the Oceans 2012 MTS/IEEE Hampton Roads Conference & Exhibition. OCEANS MTS/IEEE Conference (OCEANS-2012), October 14-19, Hampton Roads,, Virginia, USA*. o.A., 10 2012.

[4] J. Schwendner, T. M. Roehr, S. Haase, M. Wirkus, M. Manz, S. Arnold, and J. Machowinski, "The artemis rover as an example for model based engineering in space robotics," in *Workshop Proceedings of the IEEE International Conference on Robotics and Automation 2014. IEEE International Conference on Robotics and Automation (ICRA-2014), May 31 - June 7, Hong Kong, China*. IEEE, 5 2014.

[5] S. Floegel, L. Thomsen, J. Schwendner, A. Duda, T. Kwasnitschka, O. Pfannkuche, D. Wilde, R. Rosta, and A. Purser, "Temporal and spatial benthic data collection via mobile robots: present and future applications," in *Proceedings of MTS/IEEE Conference OCEANS15 Genova, Discovering Sustainable Ocean Energy for a New World. To appear.*, 2015.

[6] M. Hildebrandt and J. Hilljegerdes, "Design of a versatile auv for high precision visual mapping and algorithm evaluation," in *2010 IEEE/OES Autonomous Underwater Vehicles (AUV). IEEE/OES Autonomous Underwater Vehicles (AUV-2010), Mapping the Worlds Oceans, September 1-3, Monterey,, CA, USA*, IEEE/OES. IEEE, 2010.

[7] M. Hildebrandt, C. Gaudig, L. Christensen, S. Natarajan, P. M. Paranhos, and J. Albiez, "Two years of experiments with the auv dagon - a versatile vehicle for high precision visual mapping and algorithm evaluation," in *Proceedings of IEEE/OES Autonomous Underwater Vehicles. IEEE/OES Autonomous Underwater Vehicles (AUV-2012), September 24-27, Southampton, United Kingdom*. o.A., 9 2012.

[8] J. Albiez, S. Joyeux, C. Gaudig, J. Hilljegerdes, S. Kroffke, C. Schoo, S. Arnold, G. Mimoso, P. Alcantara, R. Saback, J. Neto, D. Cesar, G. Neves, T. Watanabe, P. Merz Paranhos, M. Reis, and F. Kirchner, "FlatFish – a compact subsea-resident inspection auv," in *Proceedings of the MTS/IEEE OCEANS 2015*, Washington DC, USA, Oct 2015, pp. 1–8.

[9] Chulliat, A., S. Macmillan, P. Alken, C. Beggan, M. Nair, B. Hamilton, A. Woods, V. Ridley, S. Maus, and A. Thomson, "The us/uk world magnetic model for 2015-2020," NOAA National Geophysical Data Center, Boulder, CO, Tech. Rep., 2015.

[10] C. C. Finlay, S. Maus, C. D. Beggan, T. N. Bondar, A. Chambodut, T. A. Chernova, A. Chulliat, V. P. Golovkov, B. Hamilton, M. Hamoudi, R. Holme, G. Hulot, W. Kuang, B. Langlais, V. Lesur, F. J. Lowes, H. Lühr, M. M. S. Macmillan, S. McLean, C. Manoj, M. Menvielle, I. Michaelis, N. Olsen, J. Rauberg, M. Rother, T. J. Sabaka, L. T.-C. A. Tangborn, E. Thébault, A. W. P. Thomson, I. Wardinski, Z. Wei, and T. I. Zvereva, "International geomagnetic reference field: the eleventh generation," *Geophysical Journal International*, vol. 183, pp. 1216–1230, 2010.

[11] G. A. Glatzmaier and P. H. Roberts, "A three-dimensional self-consistent computer simulation of a geomagnetic field reversal," *Nature*, vol. 377, no. 6546, pp. 203–209, Sep 1995.

[12] M. Caruso, "Applications of magnetic sensors for low cost compass systems," in *Position Location and Navigation Symposium, IEEE 2000*, 2000, pp. 177–184.

[13] A. Banerjee, I. S. Dhillon, J. Ghosh, and S. Sra, "Clustering on the unit hypersphere using von mises-fisher distributions," in *Journal of Machine Learning Research*, 2005, pp. 1345–1382.

[14] S. Sra, "A short note on parameter approximation for von mises-fisher distributions: and a fast implementation of i s (x)," *Computational Statistics*, vol. 27, no. 1, pp. 177–190, 2012.